arXiv:1412.2740v1 [astro-ph.GA] 8 Dec 2014

# Origin of Hydrogen Ionization in the 1 pc Galactic Central Region

D.O. Chernyshov[a,b,*], Gene C.K. Leung[b], K.S. Cheng[b], V.A. Dogiel[a,b,c], V. Tatischeff[d]

[a] *I.E.Tamm Theoretical Physics Division of P.N.Lebedev Institute of Physics, Leninskii pr. 53, 119991 Moscow, Russia*
[b] *Department of Physics, University of Hong Kong, Pokfulam Road, Hong Kong, China*
[c] *Moscow Institute of Physics and Technology, 141700 Moscow Region, Dolgoprudnii, Russia*
[d] *Centre de Sciences Nucléaires et de Sciences de la Matiére, IN2P3/CNRS and Univ Paris-Sud, 91405 Orsay Campus, France*

**Abstract**

We study a possible connection between processes of gamma-ray emission and hydrogen ionization in a few pc of central region around Sgr A*. Previous investigations showed there is a discrepancy between interpretation of gamma-ray and ionization data if gamma-rays are generated by proton-proton collisions. Here we provided analysis of processes of ionization and emission basing on analytical and numerical calculations of kinetic equations which describe processes of particle propagation and their energy losses. We assumed that cosmic rays (CRs) are emitted by a central source. The origin of gamma rays could be either due to collisions of relativistic protons with the dense gas of the surrounding circumnuclear disk (CND) or bremsstrahlung and inverse Compton scattering of relativistic electrons. The hydrogen ionization in this case is produced by a low energy component of the CR spectrum. We found that if ionization is produced by protons the expected ionization rate of hydrogen in the CND is of the same order as derived from IR observations. So we do not see any discrepancy between the gamma-ray and ionization data for the hadronic model. In the case of ionization by electrons we obtained the ionization rate one order of magnitude higher than follows from the IR data. In principle, a selection between the leptonic and hadronic interpretations can be performed basing on measurements of radio and X-ray fluxes from this region because the leptonic and hadronic models give different values of the fluxes from there. We do not exclude that gamma-ray production and hydrogen ionization in the CND are due to a past activity of Sgr A* which occurred about 100 year ago. Then we hypothesize that there may be connection between a past proton eruption and a flux of hard X-rays emitted by Sgr A* hundred years ago as follows from the observed time variability of the iron line seen in the direction of GC molecular

*Corresponding author
*Email address:* chernyshov@dgap.mipt.ru (D.O. Chernyshov)

clouds.

*Keywords:* Galaxy: center, cosmic rays, gamma rays: general

## 1. Introduction

The central region around Srg A* of the radius about several pc is characterized by very peculiar parameters of the interstellar medium (see e.g. Ferrière et al., 2007; Ferrière, 2012). The central black hole is surrounded by the circumnuclear disk (CND) whose total mass was estimated by Christopher et al. (2005) as $10^6 M_\odot$. The analysis performed by Ferrière (2012) gives a slightly lower value of $\sim 2 \times 10^5 M_\odot$ for the region of radius $R_c = 3 - 5$ pc that gives the average gas density in the CND of about $n_H \simeq 4 \times 10^5$ cm$^{-3}$.

Recent observations of the The High Energy Stereoscopic System (H.E.S.S.) (Aharonian et al., 2009) and *Fermi* Large Area Telescope (*Fermi* LAT) gamma-ray telescopes (see Chernyakova et al., 2011) found a prominent gamma-ray flux in the TeV and GeV regions (the source 2FGL J1745.6−2858 in the second *Fermi* LAT source catalog (see Nolan et al., 2012)) that indicated that this region is filled with high energy cosmic rays (CRs). The estimated gamma-ray flux from 2FGL J1745.6−2858 for $E > 2$ GeV is about $I_{obs} = 1.08 \times 10^{-10}$ erg cm$^{-2}$s$^{-1}$ with the spectral index $\gamma = 2.68$ (see Chernyakova et al., 2011) that corresponds a luminosity about $8 \times 10^{35}$ erg s$^{-1}$. In Fig. 1 the CND region is shown by the red circle. The position of Sgr A* is shown by the black cross. Positions of IR sources used by Goto et al. (2013) are shown in Fig. 1 by the green circle. The 95% confidence positional error circle of 2FGL J1745.6−2858 is labeled with a black circle. The molecular complexes CND, 20 km/s, 50 km/s and the SNR Sgr A East are also shown in the figure. We derived the 95% confidence positional error circle for *Fermi* LAT data collected in the time interval from August 4, 2008 to May 30, 2014. The data were reduced and analyzed using the *Fermi* Science Tools package (v9r32p5), available from the *Fermi* Science Support Center [1].

Additional evidence for CRs in the GC was obtained by Goto et al. (2013, 2014) who estimated the rate of hydrogen ionization in the GC from observations of IR absorption lines in spectra of several sources. Positions of IR sources used by Goto et al. (2013) are shown in Fig. 1 by the green circle. Goto et al. (2013) estimated the ionization rate in the 1 pc region of the CND as $\zeta \simeq 1.2 \times 10^{-15}$ s$^{-1}$ which is of the order of the ionization rate derived for the more extended central region of radius $\sim 100$ pc (see, e.g., Oka et al., 2005). It was concluded that the ionization in the 100 pc region is mainly produced by subrelativistic CRs whose source luminosity in the GC is no more than $10^{38} - 10^{39}$ erg s$^{-1}$ (see, e.g., Dogiel et al., 2013, 2014; Yusef-Zadeh et al., 2013).

As seen from observations, the positional error circle of 2FGL J1745.6−2858 overlaps with the CND, which is compatible with the picture that its emission

[1] http://fermi.gsfc.nasa.gov/ssc/data/analysis/software/

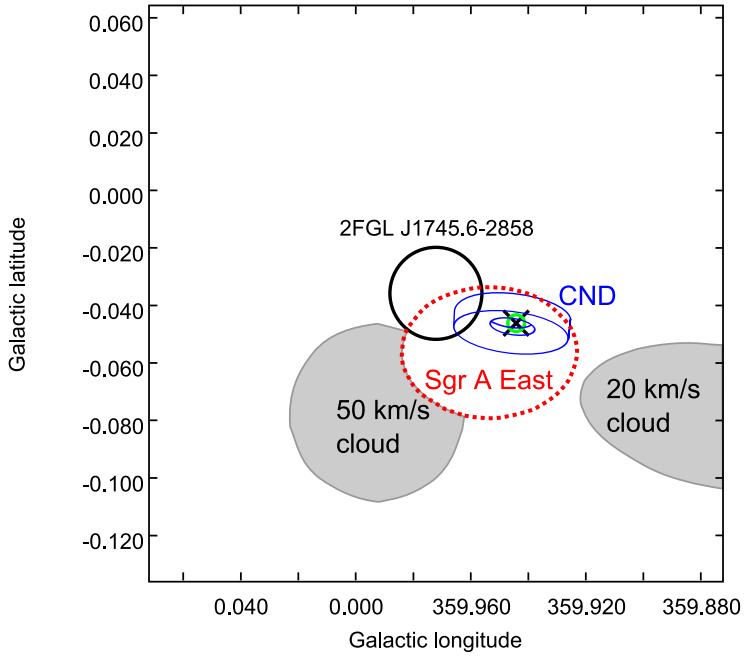


Figure 1: Positions of sources within the $0°.2 \times 0°.2$ region centered at 2FGL J1745.6−2858. The 95% confidence positional error circle of 2FGL J1745.6−2858 in 2FGL is labeled with a black circle, the position of Sgr A* with a black cross and the position of the IRS stars with a green circle. The molecular complexes CND, 20 km/s and 50 km/s (see Ferrière, 2012) are also shown in the figure.

originates within the CND. It is reasonable to assume that this emission is provided by CRs emitted by Sgr A* as assumed by Chernyakova et al. (2011). The energy release in Sgr A* may be large enough to produce this gamma-ray flux. Thus, Yusef-Zadeh et al. (2012) concluded from high resolution X-ray and radio data within 5 pc central region that Sgr A* released energy during the last 1-3 hundred years in the form of a jet with the gamma factor $\gamma \sim 3$. The estimated outflow kinetic luminosity is about $1.2 \times 10^{41}$ erg s$^{-1}$.

Goto et al. (2013) analyzed whether the hydrogen ionization can be provided by CR protons which also generate there the observed gamma-ray flux. The proton spectrum at $E > 1$ GeV at the Galactic center was derived by Chernyakova et al. (2011) in the assumption that the gamma-ray flux from the source 2FGL J1745.6−2858 was produced by proton-proton $(p-p)$ collisions in the 3 pc CND region where the gas density equaled $\bar{n}_H = 10^3$ cm$^{-3}$. Our estimations show, that if the spectrum is as derived by Chernyakova et al. (2011), the ionization rate produced by relativistic protons only with $E > 1$ GeV is about $10^{-14}$ s$^{-1}$, i.e. one order of magnitude higher than the values of Goto et al. (2013) obtained from the IR observations.

Goto et al. (2013) assumed that if this spectrum can be extrapolated into

the range $E < 1$ GeV, the expected ionization rate, produced by subrelativistic protons, was four orders of magnitude higher than that deduced from the $H_3^+$ observations.

All of these lead to a strong discrepancy between the observed ionization rate within the CND region and the hadronic model of gamma-rays in the CND region.

Below we re-analyze the origin of GeV gamma rays and the hydrogen ionization in the CND in order to find an alternative explanation of this discrepancy.

We re-analyze processes of ionization and gamma-ray production in the CND for the hadronic and leptonic models, namely:

- We assume that CRs are emitted in the CND by a central source which can be either Sgr A* or any SNR e.g. Sgr A East;
- Ionization and gamma rays are produced by CR protons. In this case gamma-ray photons are generated by $p - p$ collisions;
- Ionization and gamma rays are produced by CR electrons. In this case gamma-ray photons are produced by bremsstrahlung and inverse Compton scattering. The inverse Compton model of gamma-ray emission from the Sgr A* was presented e.g. in Kusunose & Takahara (2012).

Unlike previous investigations we derive the spectrum of emitting particles in the relativistic and subrelativistic energy ranges from corresponding kinetic equations which include processes of energy losses and, if necessary, particle propagation. The parameters of CND region were taken from Ferrière (see 2012). The strength of magnetic field around Sgr A* and in the CND is about $(1 - 4) \times 10^{-3}$ G (see Killeen et al., 1992; Yusef-Zadeh et al., 1996; Eatough et al., 2013), and the density of background photons (IR and optical) $w_{ph} \sim 10^4$ eV cm$^{-3}$ (see Mezger et al., 1996).

## 2. *Fermi* LAT observations

Previous *Fermi* LAT observations (e.g. Chernyakova et al., 2011; Nolan et al., 2012) on this source made use of 2 years of data. Now with 6 years of *Fermi* LAT data available, it is useful to perform an up-to-date analysis to benefit from the increased statistics. For $\gamma$-ray observation, we used *Fermi* LAT data collected in the time interval from August 4, 2008 to May 30, 2014. The data was reduced and analyzed using the *Fermi* Science Tools package (v9r32p5), available from the *Fermi* Science Support Center [2]. We selected events in the reprocessed Pass 7 'Source' class and used the P7REP_SOURCE_V15 version of the instrument response functions. To reduce contamination from the gamma-rays produced in the upper atmosphere, we excluded time intervals when the region of interest (ROI) was observed at zenith angles greater than 100° or when

[2] http://fermi.gsfc.nasa.gov/ssc/data/analysis/software/

the rocking angle of the LAT was greater than 52°. We used photons between 0.1 and 300 GeV within a 20° × 20° ROI centered at the position of 2FGL J1745.6-2858.

We performed a binned likelihood analysis with the gtlike tool. For source modeling, all 2FGL catalog sources (Nolan et al., 2012) within 19° of the ROI center, the galactic diffuse emission (gll_iem_v05.fits) and isotropic diffuse emission (iso_source_v05.txt) were included. For sources more than 10° away from the ROI center, all spectral parameters were fixed to the catalog values. We modeled 2FGL J1745.6-2858 with a log-parabola function as in the 2FGL catalog

$$\frac{dN}{dE} = N_0 \left(\frac{E}{E_0}\right)^{-(\alpha+\beta\log(E/E_0))} . \quad (1)$$

Spectral points were obtained by fitting the normalization factors of point sources within 3° from the source of interest and the diffuse backgrounds in individual energy bins. Other parameters were fixed to the best-fit values found in the full energy band fit. In each energy bin, an initial fit was performed using the DRMNFB optimizer, which has a weaker convergence criterion. We identified and removed all point sources with TS values $< 0$ in that energy bin, and re-optimized the fit using the NEWMINUIT optimizer, which has a stricter convergence criterion.

We note that the Galactic Center region has a strong diffuse emission background and a high density of point sources. A total of 10 2FGL sources are located within 2° from the galactic center, and the nearest source 2FGL J1746.6-2851c and 2FGL J1747.3-2858c are located only 0°.25 and 0°.66 from the source of interest. This leads to a possibility of background confusion, which affects the lowest energy band most severely due to the large point spread function of the LAT at $\sim$ 100 MeV.

We investigated the effect of the background confusion in the 100-158 MeV energy bin by performing two separate fits where the the fluxes of 2FGL J1746.6-2851c and 2FGL J1747.3-2858c were fixed to the lower and upper bounds obtained in the full energy fit, respectively. The resulting fluxes were $\sim$ 20% lower than that obtained in a simple fit. We adopted these two values as the lower and upper bounds of the flux in 100-158 MeV.

Figure 1 shows the positions of the sources in a $0°.2 \times 0°.2$ region centered at the position of 2FGL J1745.6-2858. The 95% confidence positional error circle of 2FGL J1745.6-2858 from the catalog and the size of the circumnuclear disk are shown in the Figure (see figure captions). The overlap between the source and the circumnuclear disk shows that the emission may originate within the CND.

The spectrum of the gamma-ray emission is presented in Section 5. For comparison we also plotted in this figure the data from Chernyakova et al. (2011) and from 2FGL. Our spectrum agrees with 2FGL in general, but the increased statistics allowed for smaller error bars and finer binning in energy, which could put better constraint for various models.

## 3. Kinetic equation for CRs in the CND region

The general kinetic equation for CRs can be presented in the form

$$\frac{\partial N}{\partial t} - \nabla(D\nabla N) + \frac{\partial}{\partial E}\left(\frac{dE}{dt}N\right) + \frac{N}{T} = Q(E, r, t) \tag{2}$$

where $N(E)$ is the CR density, $E$ is the particle energy, $dE/dt$ is the rate of energy losses for protons or electrons, $Q(E)$ is the source function, $T$ is the particle lifetime, which e.g. for protons is the time of $p-p$ collisions, and $D$ is an affective diffusion coefficient due to scattering on magnetic fluctuations (see e.g. Berezinskii et al., 1990).

If a point-like source emits a power-law momentum spectrum of particles ($\propto p^{-\gamma}$) with the spectral index $\gamma$ then its energy spectrum can be presented as

$$Q(r, E, t) = A(E, t)\delta(\mathbf{r}) \tag{3}$$

with

$$A(E) = A_0(t)\frac{E + Mc^2}{(E^2 + 2Mc^2E)^{(\gamma+1)/2}} \tag{4}$$

Here $M$ is the particle mass, $E$ its energy, $\gamma$ is the injection spectral index of protons and $A_0$ is proportional to the source power.

In the non-relativistic energy range the injection spectrum is transformed by ionization losses. The rate of ionization losses is (Hayakawa, 1964; Ginzburg, 1989)

$$\left(\frac{dE}{dt}\right)_i = -\frac{2\pi e^4 n_H}{m_e c\beta(E)} \ln\left(\frac{m_e^2 c^2 W_{max}}{4\pi e^2 \hbar^2 n}\right) \tag{5}$$

where $n_H$ is the density of background gas, $m_e$ is electron mass, $W_{max}$ is the highest energy transmitted to an ambient electron, and $\beta(E) = v/c$. The accurate expression for energy losses at low energies was taken from the PSTAR and ESTAR database (see Berger et al. , 2005) for protons and electrons, for electron energies below 10 keV we used the approach of Dalgarno et al. (1999).

The process of catastrophic $p-p$ collisions can be presented as continuum energy losses, and the approximate formula for $p-p$ energy losses can be given as (see Mannheim & Schlickeiser, 1994),

$$\left(\frac{dE}{dt}\right)_{pp} = -0.65cn_H\sigma_{pp}\theta\left(E - 1.22 \text{ GeV}\right) , \tag{6}$$

where $\sigma_{pp}$ is the cross-section of proton-proton collisions. Thus for protons

$$\frac{dE}{dt} = \left(\frac{dE}{dt}\right)_{pp} + \left(\frac{dE}{dt}\right)_i . \tag{7}$$

As one can see from Eq. (2) the problem is characterized by the three times which for the CND parameters are:

- The characteristic time of $p-p$ collisions

$$\tau_{pp} = n_H c \sigma_{pp} \simeq 100 \text{ yr}\,; \tag{8}$$

- The characteristic time of ionization losses

$$\tau_i = \int\limits_E \frac{dE}{(dE/dt)_i} \text{ yr}\,, \tag{9}$$

  that gives $\tau_i \simeq 10^3 \left(\frac{1\ GeV}{E}\right)^{3/2}$ yr for subrelativistic protons;

- The characteristic time of diffusion

$$\tau_D \simeq \frac{R^2}{4D}\,, \tag{10}$$

  where $R \simeq 3$ pc is the size of the CND region.

Depending of relations between these characteristic times different spectra of CRs can be generated in the CND.

We notice that the value of diffusion coefficient $D$ in the CND is, of course, unknown. The two limit cases are possible. As it was shown by Kulsrud & Pearce (1969) magnetic fluctuations are damped in a dense gas of molecular clouds because of ion-neutral friction, that gives free CR escape from the clouds. On the other hand, a neutral gas in the clouds is turbulized. This turbulence excites forced magnetic fluctuations. As a result a spagetti like structure of magnetic field line is generated inside the clouds and the energy of magnetic fluctuations is concentrated at a small correlation length of the magnetic field, $L_{corr}$, which is much smaller than a size of the molecular cloud (see Dogiel et al., 1987, 2014; Istomin & Kiselev, 2013). These fluctuations prevent free escape of CRs from the clouds. As a result magnetized particles propagate along tangled magnetic field lines that can be described by diffusion with the coefficient

$$D \sim \beta \frac{c L_{corr}}{3}\,, \tag{11}$$

where $L_{corr}$ is the correlation length of turbulized magnetic field, and $\beta = v/c$. Below we estimate the value of $D$ from solutions of kinetic equations and observational data.

## 4. Processes of ionization and emission in the CND

For the hadronic origin of the CND gamma rays, their flux from the CND is

$$F_\gamma(E_\gamma, t) = \frac{n_H c}{R_{GC}^2} \int\limits_0^R r^2 dr \int_E N(E, r, t) \frac{d\sigma}{dE_\gamma}(E, E_\gamma) dE\,, \tag{12}$$

where $n_H$ is the average hydrogen density in the gamma-ray emitting region, $V$ is its volume, $R_{GC} = 8$ kpc is the distance from Earth to the CND, and $d\sigma/dE_\gamma(E, E_\gamma)$ is the differential cross-section for gamma-ray production in proton-proton collisions (Kamae et al., 2006).

In the case of leptonic origin, gamma rays can be generated by the bremsstrahlung in the CND gas and/or by the inverse-Compton scattering of electrons on background photons,

$$F_\gamma(E_\gamma) = \frac{n_H c}{R_{GC}^2} \int_0^R r^2 dr \int N_e(E, r, t) \left(\frac{d\sigma}{dE_\gamma}\right)_{br} dE + \frac{c}{R_{GC}^2} \int_0^R r^2 dr \int N_e(E, r, t) dE \int w(\epsilon, r) \left(\frac{d\sigma}{dE_\gamma}\right)_{IC} d\epsilon \,, \tag{13}$$

where $\left(\frac{d\sigma}{dE_\gamma}\right)_{IC}$ and $\left(\frac{d\sigma}{dE_\gamma}\right)_{br}$ are the differential cross-section of inverse-Compton and bremsstrahlung processes accordingly (see Blumenthal & Gould , 1970), $\epsilon$ is the energy of soft photons (IR and optical) and $w(\epsilon)$ is their energy density.

The ionization rate of hydrogen by the protons or electrons in this region can be estimated from

$$\zeta = \int \sigma_H v N(E) dE \,, \tag{14}$$

where $\sigma_H$ is the ionization cross-section of the molecular hydrogen by proton or electron impact whose equation is approximately (see Spitzer & Tomasko, 1968)

$$\sigma_H = 1.23 \times 10^{-20} \frac{1}{\beta^2} \left[6.2 + \lg\left(\frac{\beta^2}{1-\beta^2}\right) - 0.43\beta^2\right] \mathrm{cm}^2 \tag{15}$$

for more accurate equations of cross-section (see Rudd et al., 1983; Tatischeff, 2003).

Protons produce also secondary electrons and positrons by $p - p$ collisions and by the knock-on process. The production rate of secondary electrons is estimated as

$$Q_e(E_e, \mathbf{r}, t) = n_H \int N(E, \mathbf{r}, t) v(E) \frac{d\sigma}{dE_e} dE \,, \tag{16}$$

where $\frac{d\sigma}{dE_e}$ is the differential cross-section for electron and positron production. For the $p - p$ process the cross-section is presented in e.g. Kamae et al. (2006). The knock-on cross-section has the approximated form as (see e.g. Ginzburg, 1989)

$$\frac{d\sigma}{dW} \simeq \frac{2\pi e^4}{m_e v^2 W^2} \tag{17}$$

where $v$ and $W$ are the velocity of a primary particle and the energy of a secondary electron, respectively. For more accurate equations for the cross-section see Daniel & Stephens (1975) and Hayakawa (1964).

The spectrum of secondary electrons in the CND is calculated from Eq. (2) for $Q(E_e)$ in the form (16).

Relativistic electrons generate radio emission by the synchrotron losses. The corresponding equation for synchrotron emission is (see for details Ginzburg, 1989)

$$\Phi(\nu,t)=\frac{\sqrt{3}e^3H}{m_ec^2R_{GC}^2}\int\limits_0^R r^2dr\int\limits_0^{E_{max}}N(E_e,r,t)dE_e\frac{\nu}{\nu_c}\int\limits_{\nu/\nu_c}^{\infty}K_{5/3}(x)dx \qquad (18)$$

where $N(E_e)$ is the density of electrons with the energy $E_e$, $K_\alpha(x)$ is the McDonald function and $\nu_c=3eH\gamma^2/4m_ec$, $\gamma$ is the Lorenz-factor of an electron.

Subrelativistic electrons and protons produce bremsstrahlung X-ray emission. The equation for the bremsstrahlung radiation is

$$F_{br}(E_x,t)=\frac{n_H}{R_{GC}^2}\int\limits_0^R r^2dr\int N(E,r,t)v(E)\left(\frac{d\sigma}{dE_x}\right)_{br}dE\,, \qquad (19)$$

where

$$\left(\frac{d\sigma}{dE_x}\right)_{br}=\frac{8}{3}\frac{e^2}{\hbar c}\left(\frac{e^2}{m_ec^2}\right)^2\frac{m_ec^2}{\hat{E}E_x}\ln\left[\frac{(\sqrt{\hat{E}}+\sqrt{\hat{E}-E_x})^2}{E_x}\right] \qquad (20)$$

Here $\hat{E}=E_e$ for electrons and $\hat{E}=(m_e/m_p)E_p$ for protons, where $m_p$ is the mass of the proton.

## 5. Steady State Hadronic Model

We start from the simplest case of steady state model for protons. If the mean path length of protons equals or is longer than the CND radius, $\sqrt{D\tau_{pp}}\geq R$ then we can use equation for the total number of protons $\bar{N}(E)=\int\limits_0^R r^2drN(E,r)$ in the CND. In this case the equation for the particle number $\bar{N}$ reads as

$$\frac{d}{dE}\left(\frac{dE}{dt}\bar{N}\right)=\bar{Q}(E) \qquad (21)$$

where the energy loss term is taken in the form (7), and $\bar{Q}(E)$ in the form (3). The solution of Eq. (21) is

$$\bar{N}(E)=\frac{1}{dE/dt}\int\limits_E^{\infty}\bar{Q}(E)dE\,. \qquad (22)$$

As in Eq.(12) the flux of gamma rays with the energy $E_\gamma$ from the CND is

$$F_\gamma(E_\gamma)=\frac{M_Hc}{4\pi R_{GC}^2m_p}\int\frac{\bar{N}(E)}{V}\frac{d\sigma}{dE_\gamma}(E,E_\gamma)dE\,, \qquad (23)$$

where $V$ is the CND volume, $M_H$ is the total mass of hydrogen there.

We assume that the gamma-ray flux from the source 2FGL J1745.6−2858 is generated within the CND region. Then the results depend only on the total mass of the hydrogen within the area covered by relativistic proton. The average spectrum of CR protons $\bar{N}(E)/V$ derived for the total mass of the CND and the gamma-ray flux of J1745.6−2858 is shown in Fig. 2. From this figure one can see that the derived density of protons is below the estimates of Chernyakova et al. (2011) in the relativistic energy range and strongly below the approximation of Goto et al. (2013) because of the ionization losses.

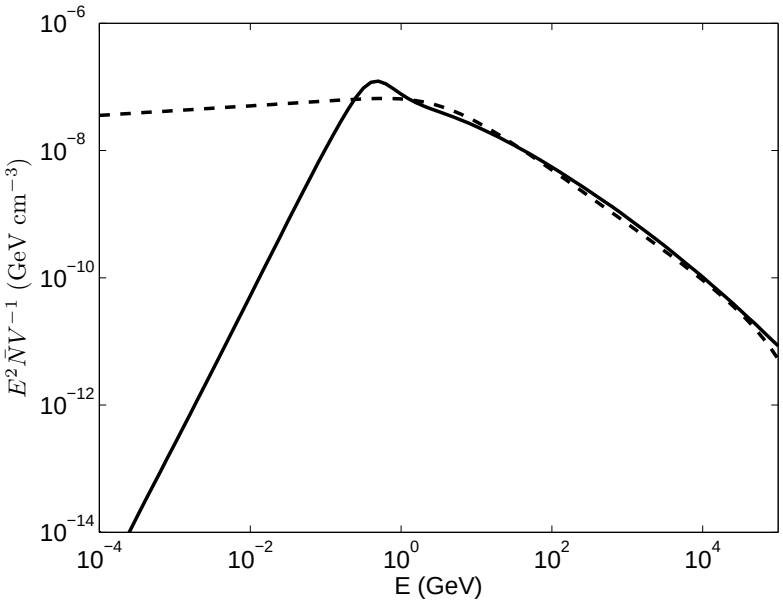


Figure 2: The energy spectrum of protons (solid line) derived from Eq. (22) and the data of Chernyakova et al. (2011) and Ferrière (2012). The injection spectrum is shown by the dashed line.

The calculated gamma-ray spectrum produced by these protons is shown in Fig. 3 by solid line.

For this spectrum of protons we can calculate from Eq. (16) the production rate of secondary electrons. In the steady state case the total number of secondary electrons can be estimated as

$$\bar{N}_e^{sec}(E_e) = \frac{1}{dE/dt} \int_{E_e}^{\infty} \bar{Q}_e(E) dE \,, \tag{24}$$

where the term $dE/dt$ describes the total energy losses of electrons, which includes the ionization, bremsstrahlung, synchrotron and inverse-Compton losses.

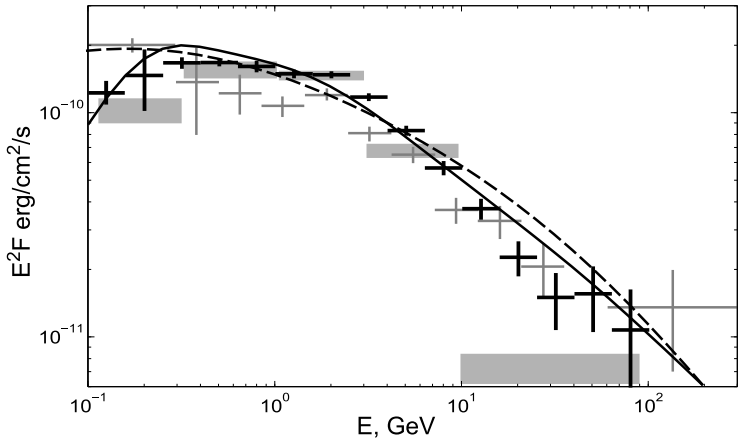


Figure 3: Gamma-ray spectrum expected in the case of hadronic origin of the gamma-ray emission (solid line) and in the case of leptonic origin of the gamma-ray emission (dashed line). Data points in form of gray crosses are from Chernyakova et al. (2011), data points in form of gray bars are from the second Fermi catalog and data points in form of black crosses are from this work.

The contribution of secondary electrons to the total gamma-ray flux from the CND is relatively low. However, these electrons emit a flux of radio emission from the CND region. The radio spectrum in the CND is calculated from Eq. (18) and (24) and it is shown in Fig. 4 by the heavy solid line. The estimated radio flux at $\nu = 1.5$ GHz is about 4.63 Jy.

The ionization rate of hydrogen by the protons in the stationary model can be approximated as

$$\zeta = \int \sigma_H v \frac{\bar{N}(E)}{V} dE \,. \tag{25}$$

Our can calculations show that the ionization rate is about $4.6 \times 10^{-15}\mathrm{s}^{-1}$, of which $2.85 \times 10^{-15}\mathrm{s}^{-1}$ is produced by primary protons and $1.75 \times 10^{-15}\mathrm{s}^{-1}$ by secondary electrons.

From Eq.(19) we calculated X-rays flux in the range 20-40 keV generated by bremsstrahlung of protons and electrons. The total flux is about $3.1 \times 10^{-13}$erg cm$^{-2}$s$^{-1}$ , protons generate $2.27 \times 10^{-13}$erg cm$^{-2}$s$^{-1}$ and secondary electrons - $0.83 \times 10^{-13}$erg cm$^{-2}$s$^{-1}$. The spectral index of bremsstrahlung radiation in this range is $-1.53$.

## 6. Transient Injection of Protons

Here we investigate another limit case of proton injection, namely the case of transient injection. As in Chernyakova et al. (2011) we assume that the injection of protons happened $t$ years ago, and the gamma-ray flux from the CND at present is just as observed from 2FGL J1745.6−2858.

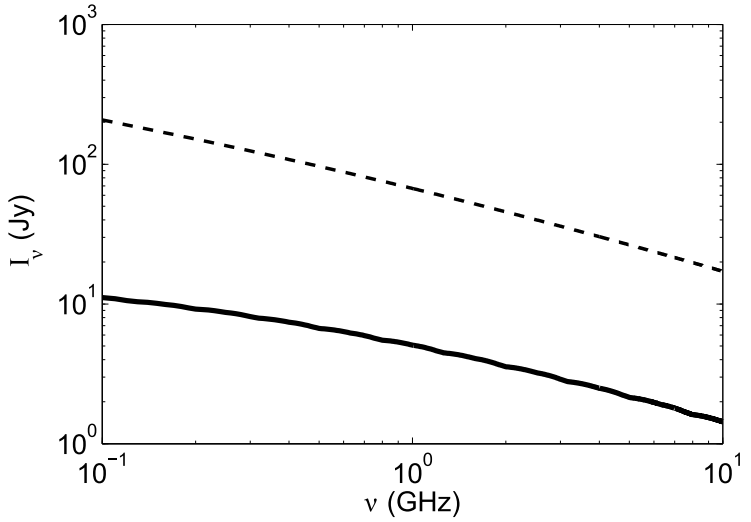


Figure 4: Radio emission expected in the case of hadronic (solid line) and leptonic (dashed line) origin of the gamma-ray emission.

For the transient injection the source function $Q(E, r, t)$ is taken in the form

$$Q(E, r, t) = A(E)\delta(\mathbf{r})\delta(t) \tag{26}$$

where $A(E)$ is given by Eq. (4) that gives $A(E) = A_0 E^{-\gamma}$ in the relativistic energy range, and $A(E) = A'_0 E^{-(\gamma+1)/2}$ in the subrelativistic energy range.

Using the Green function of Eq.(2) as derived by Syrovatskii (1959) the spectrum can be presented as

$$N(E, r, t) = \frac{A_0 E^{-\gamma}}{(4\pi Dt)^{3/2}} e^{-t/\tau_{pp}} \exp\left(-\frac{r^2}{4Dt}\right) \tag{27}$$

in the relativistic energy range and

$$N(E, r, t) = \frac{A'_0 \sqrt{E}}{(4\pi Dt)^{3/2}} \exp\left(-\frac{r^2}{4Dt}\right) \left(at + E^{3/2}\right)^{-(\gamma+1)/3} \tag{28}$$

in the subrelativistic energy range. Here according to Eq.(5) the rate of ionization energy losses in the subrelativistic range is presented as $dE/dt = -a/\sqrt{E}$.

We analyse the two cases when

$$\sqrt{4D\tau_{pp}} < R \quad \text{and} \quad \sqrt{4D\tau_{pp}} > R\,. \tag{29}$$

1. In the first case the protons do not leave the CND region and are absorbed there for the time $\tau_{pp}$. The diffusion coefficient in the dense CND gas is determined by a spagetti-like structure of magnetic field lines and has the

form (11), the case of Dogiel et al. (1987). As it follows from the first inequality (29), the correlation length of the magnetic field $L_{corr} < 10^{18}$ pc. The proton spectrum has a maximum in the subrelativistic energy range at (see Eq. (28))

$$E_m \simeq (at)^{2/3} \,. \tag{30}$$

where $t$ is a current time, $t < \tau_{pp}$. The evolution of proton spectrum for the diffusion coefficient $D = 3 \times 10^{27}$ cm$^2$s$^{-1}$ is shown in Fig. 5,

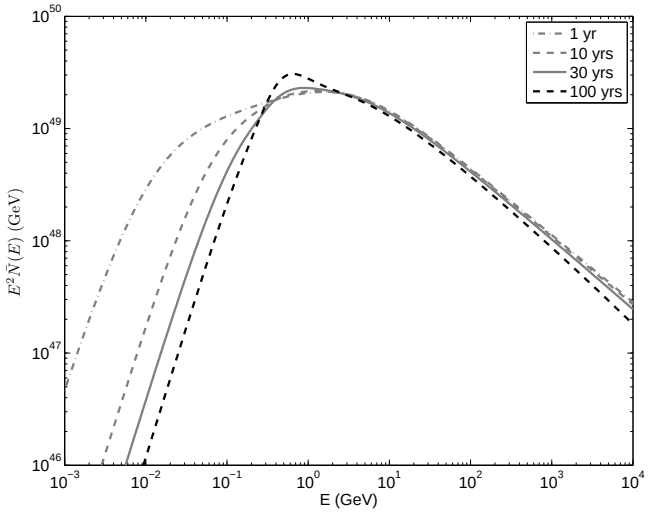


Figure 5: Evolution of the spectrum of protons injected by a point-like source. The diffusion coefficients in this case is $D = 3 \times 10^{27}$ cm$^2$s$^{-1}$.

2. In the second case a significant fraction of protons leave the CND, and only a small fraction of them interact with the CND gas. For the CND conditions this case corresponds to the inequality, $L_{corr} \geq R$. It means that CRs propagate through the CND almost without "scattering" (the case of Kulsrud & Pearce, 1969). The residence time of particles in the CND is about $R/\beta c$, which equals $\sim 10$ yr for relativistic particles. The maximum position in the proton spectrum shifts to low energies as

$$E_m \sim \left(a\frac{R}{\beta c}\right)^{2/3} . \tag{31}$$

The density of particles inside the CND is determined by particle propagation (diffusion) in the medium surrounding the CND.

As it follows from numerical calculations of Istomin & Kiselev (2013) the relation between the correlation length of magnetic fluctuations $L_{corr}$ and a size of molecular cloud depends on many parameters of the cloud, such as the

strength of large scale magnetic field, the frequency of collision between ionized and neutral particles etc.

From Eqs. (14) and (15) we calculated the ionization rate $\zeta$ in CND center for different values of $D$. The ionization rate $\zeta$ at the center of CND as a function of $t$ and $D$ is shown in Fig. 6. The gray parts of lines show parameter regions where the diffusion approximation does not work, i.e. when the lifetime of particles is shorter than the characteristic time of "scattering" by magnetic fluctuations. One can see that the calculated ionization rate is close to derived

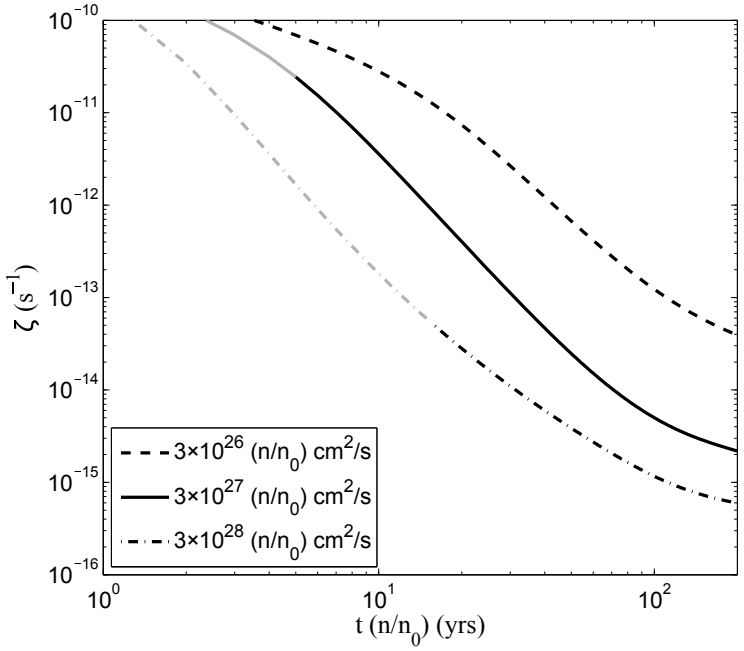


Figure 6: The ionization rate $\zeta$ at the center of CND as a function of $t$ and $D$.

by Goto et al. (2013) for the CND, $\zeta \simeq 1.2 \times 10^{-15}$ s$^{-1}$, if $D \geq 3 \times 10^{27}$ cm$^2$ s$^{-1}$. In this case a part of primary protons escape from the CND.

The total gamma-rays flux from the CND region consists of the three components, one of which is produced by $p-p$ collisions and two others by bremsstrahlung and inverse Compron losses of secondary electrons. Then from Eqs. (2), (12), (13), (16) and (27) we can estimate the energy release in the form of primary relativistic protons needed for the observed gamma-ray flux from the CND. Its value is shown in Fig. 7 for different time $t$ and different diffusion coefficients $D$.

The flux of synchrotron emission generated by secondary electrons can be calculated from Eq. (18). The flux of synchrotron radio emission from the CND region at the frequency $\nu = 1.5$ GHz for different time $t$ and different $D$ is shown in Fig. 8. An interesting characteristic of the CND radio emission is an increase

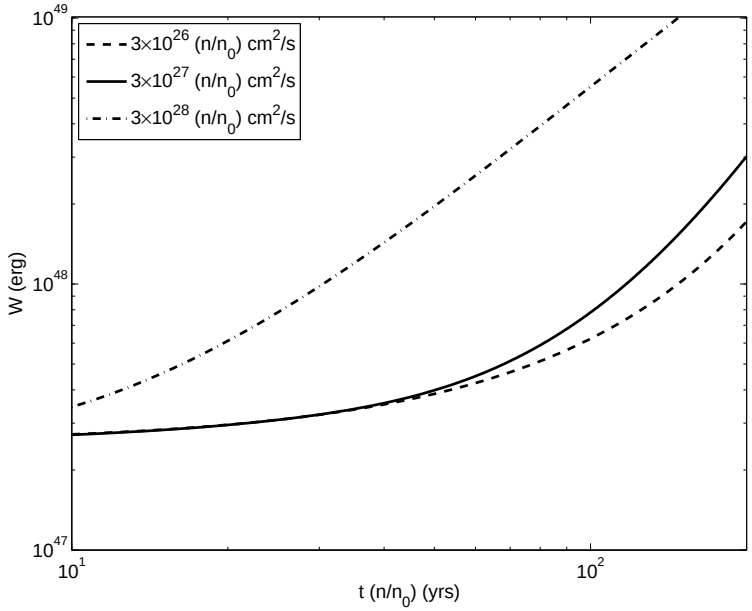


Figure 7: The energy release needed for the observed intensity of gamma-ray emission from the CND.

of the flux with time. The reason is that the lifetime of electrons emitting at the frequency 1.5 GHz is quite long, about $10^4$ yr. Therefore, for large enough $t$ and $D$ (that requires a high enough injection rate of primary protons in the past, see Fig. 7) a significant fraction of electrons, generated at initial stages, escape from the CND and form a halo around this region. Just this "old" population of electrons emitted in the past is responsible for a high radio flux observed at the current time $t$.

We expect that secondary electrons generated by proton collisions with the gas provide also a flux of X-rays from the CND. The expected flux of hard X-ray photons in the range $20 - 40$ keV is shown in Fig. 9. As one can see the flux increases also for large $t$. To interpret this effect we notice that the CND X-ray emission is generated by the three processes: by inverse bremsstrahlung of primary protons, and by bremsstrahlung and inverse Compton of secondary electrons. If the diffusion coefficient $D$ is relatively small, this emission from the CND is mainly produced by inverse bremsstrahlung of protons. However, for large enough $D$ a contribution from inverse Compton of $\sim 100$ MeV electrons which escape from the CND and fill a region around the CND, becomes significant. In this case the area of X-ray emission is more extended than the CND region.

As an example we presented spectra of X-ray components for the diffusion

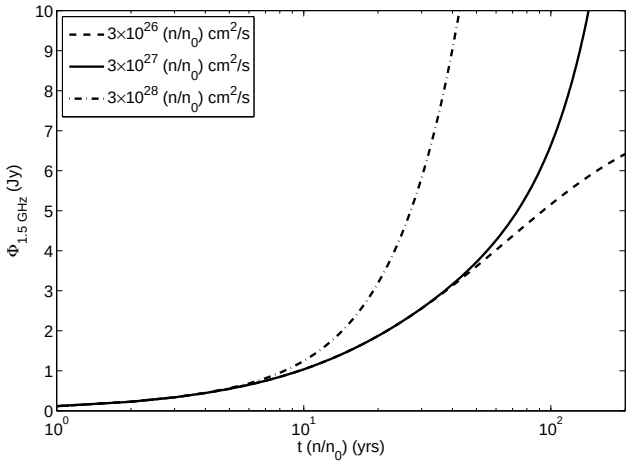


Figure 8: Synchrotron radio emission from the CND region at the frequency $\nu = 1.5$ GHz for different time momenta $t$ and different $D$.

coefficients: $D = 3 \times 10^{27}\mathrm{cm}^2\mathrm{s}^{-1}$ (Fig. 10, right panel) and $D = 3 \times 10^{28}\mathrm{cm}^2\mathrm{s}^{-1}$ (Fig. 10, left panel), the current time is $t = 100$ yr in both cases.

As it follows from our analysis the model of transient proton injection is able to reproduce characteristics of nonthermal emission from the CND and the rate of hydrogen ionization there if the proton eruption occured about hundred years ago (see e.g. Fig. 6). We notice that a high past activity of Sgr A* follows from the temporal variations of the 6.4 keV iron line observed in the direction of GC molecular clouds (see Inui et al. , 2009; Ponti et al., 2010; Terrier et al., 2010; Nobukawa et al., 2011; Clavel et al., 2013, and references therein) who found that about 100 years ago the energy release of Sgr A* was several orders of magnitude higher than at present. May it be that the gamma-ray flux from the CND, hydrogen ionization there and the time variable flux of the 6.4 keV line at present have a common origin, namely, a past activity of Sgr A*?

## 7. Hydrogen Ionization by CR Electrons

In the case of leptonic origin of gamma rays from the CND the expected ionization rate of the neutral hydrogen can be estimated in the same way as done in the previous section. The spectrum of electrons $N_e(E)$ can be estimated from Eq. (2) for the production spectrum in the form (3) and (4).

The energy loss term, $dE/dt$, includes the ionization, bremsstrahlung, synchrotron and inverse-Compton losses (see corresponding equations in Hayakawa, 1964; Ginzburg, 1989). We note that for the average density $n = 4 \times 10^5$ cm$^{-3}$, average magnetic field $H = 1$ mG and density of soft optical and IR photons $w_{op} = w_{IR} = 10^4$ eV/cm$^3$, the bremsstrahlung losses dominate up to ener-

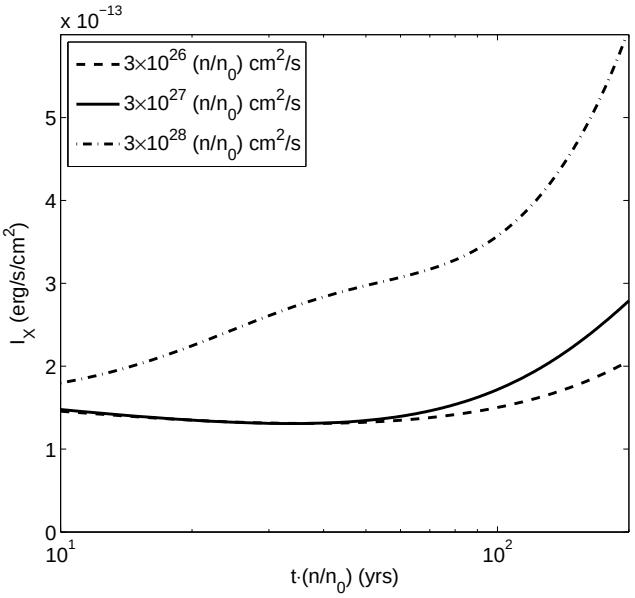


Figure 9: X-ray emission from the CND region in the range $20 - 40$ keV for different time momenta $t$ and different $D$.

gies about of 25 GeV. For the ionization losses we used the ESTAR database (Berger et al. , 2005) which provided the data up to 10 keV electron energy. Below 10 keV we used the approach for ionization losses from Dalgarno et al. (1999).

In the case of leptonic origin gamma rays can be generated by bremsstrahlung in the interstellar gas and/or by inverse-Compton scattering of electrons on background photons, as described by Eq. (13).

For observed gamma-ray flux of the source 2FGL J1745.6−2858 we derived from Eq. (13) the electron spectrum, and estimated the hydrogen ionization rate provided by these electrons in the CND.

The gamma-ray spectrum derived from the leptonic model is shown in Fig. 3 by dashed line. For the accepted parameters gamma rays are mostly produced by bremsstrahlung. The ionization rate provided by the electrons is $6.3 \times 10^{-14}$ $s^{-1}$. One can see that the ionization rate expected in the leptonic mode is higher than derived by Goto et al. (2013) from the $H_3^+$ data, $1.2 \times 10^{-15}$ $s^{-1}$. This circumstance makes the leptonic interpretation problematic, unless the electrons providing the gamma rays and the hydrogen ionization have different origin.

The estimated X-ray flux from the CND generated by the electron bremsstrahlung is about $5.5 \times 10^{-12}$ erg $cm^{-2}s^{-1}$ in the range $20 - 40$ keV. The spectral index of this emission is -1.37.

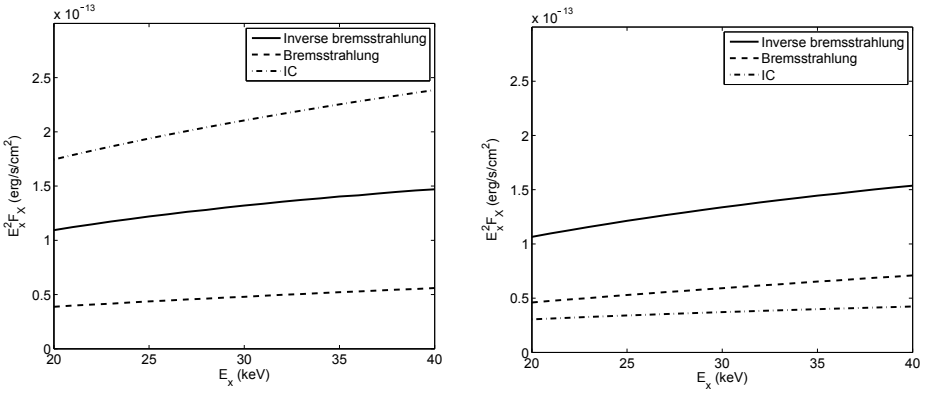


Figure 10: Components of X-ray emission at the time $t = 100$ yr for the diffusion coefficient: $D = 3 \times 10^{28}\mathrm{cm}^2\mathrm{s}^{-1}$ (left panel), and $D = 3 \times 10^{27}\mathrm{cm}^2\mathrm{s}^{-1}$ (right panel)

The expected radio emission produced by these electrons from the CND region is shown in Fig. 4 by the dashed and dash-dotted lines. The value of radio flux at 1.5 GHz is 62 Jy. This value is more than one order of magnitude larger than the estimate of 5 Jy obtained by Yusef-Zadeh (2014) that also makes leptonic interpretation problematic.

## 8. Discussion

Our analysis shows that the hydrogen ionization rate derived in the framework of the stationary hadronic model of gamma rays in the CND is about the same as the value observed by Goto et al. (2013, 2014). If these gamma rays are produced by relativistic electrons, then the expected ionization rate is higher than observed. Besides, as follows from the recent analysis of the 1.5 GHz flux from the inner 2 arcmin region within Sgr A* (Yusef-Zadeh, 2014) its value is about 5 Jy, just as expected in the hadronic model. In this respect, the hadronic model looks more attractive than the leptonic model which gives at 1.5 GHz the radio flux from the CND $\geq 50$ Jy. Further analysis of the radio emission from the GC and determination of radio counterparts of the gamma-ray source may restrict the set of the models and reveal the nature of the source. We notice that radio data are decisive for the model choice because both models predict an exact number of relativistic electrons.

Parameters of ionization and emission derived in the framework of non-stionary (transient) hadronic model are time variable and depend on characteristics of Sgr A* past activity. As it follows from our analysis the ionization rate of hydrogen $\simeq 1.2 \times 10^{-15}\mathrm{s}^{-1}$ and radio flux $\sim 5$ Jy as obtained by Goto et al. (2013) and Yusef-Zadeh (2014) for the CND region can be obtained in this model if the diffusion coefficient there is about $3 \times 10^{27}$ $\mathrm{cm}^2\mathrm{s}^{-1}$ and the proton eruption occured about hundred years ago (see Figs. 6 and 8). An interesting

circumstance of the nonstationary model is a significant contribution of electrons generated at the initial stages of activity into the fluxes of radio emission and hard X-rays. The expected flux of X-rays in the energy range $20-40$ keV is about $1.5 \times 10^{-13}$ erg cm$^{-2}$s$^{-1}$ with the spectral index about -1.5. These electrons having relatively long lifetime escape from the CND region and generate in the surrounding medium radio flux by synchrotron and a flux of X-rays by inverse Compton. In this case the emission region is more extended than the CND.

It is interesting to notice that a transient release of energy by Sgr A* 100 years ago was derived from the observed temporal variations of the 6.4 keV and hard X-ray continuum fluxes in the GC region (see Inui et al. , 2009; Ponti et al., 2010; Terrier et al., 2010; Nobukawa et al., 2011, and references therein). It was concluded that just about 100 years ago Sgr A* was a source of hard X-rays with the luminosity $\sim 10^{39}$ erg s$^{-1}$. We can hypothesize that, if the transient hadronic model describes properly processes of emission and ionization in the CND, then there may be a connection between a past proton eruption and a past X-ray activity of Sgr A*.

At the end we would like to mention that new generation gamma-ray telescopes may provide more information about the source 2FGL J1745.6−2858 and resolve it with higher accuracy than the *Fermi* LAT. For example, if the telescope GAMMA-400 is able to detect the gamma-ray flux of this source, then with the claimed angular resolution about 0.01° (Galper et al., 2013a,b) it is able to resolve the source within 1.5 pc.

## Acknowledegments

The authors thank Farhad Yusef-Zadeh for his very useful comments and the unpublished radio data which we used in the paper. The authors thank Nikolay Topchiev and Sergei Suchkov for description of GAMMA-400 properties. DOC is supported in parts by the RFFI grant 12-02-31648, the LPI Educational-Scientific Complex and Dynasty Foundation. DOC and VAD acknowledge support from the RFFI grants 15-52-52004, 15-02-02358, 15-02-08143. KSC is supported by the GRF Grants of the Government of the Hong Kong SAR under HKU 7010/13P. DOC, KSC, and VAD acknowledge support from the International Space Science Institute to the International Team "New Approach to Active Processes in Central Regions of Galaxies".

## References

Aharonian, F., Akhperjanian, A. G., Anton, G. et al. 2009, A&A, 503, 817

Berezinskii, V. S., Bulanov, S. V., Dogiel, V. A., Ginzburg, V. L., & Ptuskin, V. S. 1990, *Astrophysics of Cosmic Rays*, ed. V.L.Ginzburg, (Norht-Holland, Amsterdam)

Berger, M.J., Coursey, J.S., Zucker, M.A., & Chang, J. 2005, http://physics.nist.gov/Star

Blumenthal, G. R., & Gould, R. J. 1970, Reviews of Modern Physics, 42, 237

Cheng, K. S., Chernyshov, D. O., & Dogiel, V. A. 2006, ApJ, 645, 1138

Chernyakova, M., Malyshev, D., Aharonian, F. A. et al. 2011, ApJ, 726, 60

Chernyshov, D. O., Cheng, K.-S., Dogiel, V. A. et al. 2010, MNRAS, 403, 817

Christopher M. H., Scoville, N. Z., Stolovy, S. R., & Yun, Min S. 2005, ApJ, 622, 346

Clavel, M., Terrier, R., Goldwurm, A. et al. 2013, A&A, 558, 32

Dalgarno, A., Yan, M., & Liu, W.-H. 1999, ApJS, 125, 237

Daniel, R. R. & Stephens, S. A. 1975, SSRv, 17, 45

Dogiel, V. A., Gurevich, A. V., Istomin, Ia. N., & Zybin, K. P. 1987, MNRAS, 228, 843

Dogiel, V. A., Chernyshov, D. O., Tatischeff, V. et al. 2013, ApJ, 771, L43

Dogiel, V. A., Chernyshov, D. O., Kiselev, A. M, & Cheng, K.-S. 2014, APh, 54, 33

Eatough, R. P., Falcke, H., Karuppusamy, R. et al. 2013, Nature, 501, 391

Ferrière, K., Gillard, W., & Jean, P. 2007, A&A, 467, 611

Ferrière, K. 2012, A&A, 540, 50

Galper, A. M., Adriani, O., Aptekar, R. L. et al. 2013a, arXiv:1306.6175

Galper, A. M., Adriani, O., Aptekar, R. L. et al. 2013b, Adv. Space Res. 2013, 51, 297

Ginzburg, V.L. 1989, *Applications of Electrodynamics in Theoretical Physics and Astrophysics*, Gordon and Breech Science Publication.

Glassgold, A.E., & Langer, W.D. 1974, ApJ, 193, 73

Goto, M., Indriolo, N., Geballe, T.R., Usuda, T. 2013, The Journal of Physical Chemistry A, 117, 9919

Goto, M., Geballe, T. R., Indriolo, N. et al. 2014, ApJ, 786, 96

Hayakawa, S. 1964, *Cosmic Ray Physics*, (ed R.E. Marshak), Interscience Monographs

Inui, T., Koyama, K., Matsumoto, H., & Tsuru T. Go 2009, PASJ, 61, 241

Kamae, T., Karlsson, N., Mizuno, T., et al., 2006, ApJ, 647, 692

Killeen, N. E. B., Lo, K. Y., & Crutcher, R. 1992, ApJ, 385, 58

Istomin, Ya. N. & Kiselev, A. M. 2013, MNRAS.436.2774I

Kulsrud, R. & Pearce, W. P. 1969, ApJ, 156, 445

Kusunose, M., & Takahara, F. 2012, ApJ, 748, 34

Mannheim, K., & Schlickeiser, R. 1994, A&A, 286, 983

Melia, F., Fatuzzo, M., Yusef-Zadeh, F., & Markoff, S. 1998, ApJ, 508, L65

Mezger, P. G., Duschl, W. J., & Zylka, R. 1996 A&AR, 7, 289

Nobukawa, M., Ryu, S. G., Tsuru Go, T., & Koyama, K. 2011, ApJL, 739, L52

Nolan, P. L., Abdo, A. A., Ackermann, M. et al. 2012, ApJS, 199, 31

Oka, T., Geballe, Th. R., Goto, M. et al. 2005, ApJ, 632, 882

Pedlar, A., Anantharamaiah, K. R., Ekers, R. D. et al. 1989, ApJ, 342, 769

Ponti, G., Terrier, R., Goldwurm, A. et al. 2010, ApJ, 714, 732

Ramaty, R., Kozlovky, B., & Lingenfelter, R. E. 1979, ApJS, 40, 487

Rudd, M. E, Goffe, T. V., Dubois, R. D. et al. 1983, PhysRevA, 28, 3244

Spitzer, L., & Tomasko, M. G. 1968, ApJ, 152, 971

Strong, A. W. & Moskalenko, I. V. 1998, ApJ, 509, 212

Syrovatskii, S. I. 1959, Sov.Astron., 3, 22

Tatischeff, V. 2003, "Final Stages of Stellar Evolution" (edited by C. Motch and J.-M. Hameury), EAS Publications Series (EDP Sciences: Les Ulis, France), vol. 7, pp. 79-124

Terrier, R., Ponti, G., Belanger, G. et al. 2010, ApJ, 719, 143

Yusef-Zadeh, F., Roberts, D. A., Goss, W. M. et al. 1996, ApJ, 466, L25

Yusef-Zadeh, F., Muno, M., Wardle, M., & Lis, D. C. 2007, ApJ, 656, 847

Yusef-Zadeh, F., Arendt, R., Bushouse, H. et al. 2012, ApJ, 758, L11

Yusef-Zadeh, F., Hewitt, J. W., Wardle, M. et al. 2013, ApJ, 762, 33

Yusef-Zadeh, F. 2014, private communication